RSC Advances

ROYAL SOCIETY OF CHEMISTRY

www.rsc.org/advances

The effects of hydroxyapatite nano whiskers and its synergism with polyvinylpyrrolidone on poly(vinylidene fluoride) hollow fiber ultrafiltration membranes

Xuan Zhang, Wan-Zhong Lang*, Hai-Peng Xu, Xi Yan, Ya-Jun Guo

The Education Ministry Key Laboratory of Resource Chemistry and Shanghai Key Laboratory of Rare Earth Functional Materials, Department of Chemistry and Chemical Engineering, Shanghai Normal University, 100 Guilin Road, Shanghai 200234, China

* Corresponding author. wzlang@shnu.edu.cn (W.Z. Lang); Tel: +86-21-64321951; Fax: +86-21-64321951.

Abstract

By introducing hydroxyapatite(HAP) nano whiskers as well as polyvinylpyrrolidone(PVP), the poly(vinylidene fluoride)(PVDF)/PVP/HAP hollow fiber membranes were fabricated with wet spinning method. The aqueous solution containing 90wt.% N-methyl-2-pyrrolidone(NMP) is used as bore liquid. The effects of two additives and the synergism on the morphologies, surface properties, permeation performances, antifouling ability and mechanical properties of the PVDF/PVP/HAP membranes were characterized by numerous state-of-the-art analytical techniques, and reasonably elucidated accompanying with precipitation kinetics and shear viscosity of dopes. The results show that with the addition of HAP, the finger-like structure of PVDF/PVP/HAP membranes is gradually suppressed and replaced by sponge-like structure, and the hydrophilicity is evidently improved. The hydraulic permeability J_W firstly increases from 224.2 of M-1 to 549.1 $L \cdot M^{-2} \cdot H^{-1} \cdot bar^{-1}$ by adding 1.0wt.% HAP nano whiskers of M-2, and then decreases to 425.9 and 316.3 $L \cdot M^{-2} \cdot H^{-1} \cdot bar^{-1}$ for M-3 and M-4. The rejections of three proteins and humic acid range from 31.4% to 98.4%, and slightly decrease as HAP content increases in the membranes. The mechanical properties of the membranes are markedly improved with the addition of HAP nano whiskers. The membranes containing dual additives have higher permeability and mechanical strength than those of the fibers containing either single additive, implying the synergism of them in improving membrane properties.

Key words: Poly(vinylidene fluoride) (PVDF); Hydroxyapatite(HAP); Ultrafiltration; Hollow fiber membrane; Nano whiskers

1. Introduction

The semicrystalline poly(vinylidene fluoride)(PVDF) as one good membrane material has been widely investigated owing to its good chemical resistance, mechanical properties and thermal stability[1-4]. However, the high hydrophobicity of PVDF membranes is not of practical interest because of low permeation flux and easy fouling[5]. To improve the imperfection, many attempts were devoted to modify PVDF membranes in terms of high hydrophilicity and antifouling ability by coating[6], grafting[7], blending and so on [8, 9]. Liu[1] and Kang[2] detailedly reviewed the applications, preparations and modifications of PVDF membranes. Due to its simple process, easy to control and relatively low cost, blending method is the most efficient way. Up to now, the introduction of inorganic nanofillers to modify PVDF membranes has been widely carried out. Some representative works are summarized in Table 1. By adding inorganic nanofillers such as TiO_2, Al_2O_3 SiO_2 and so on, the modified PVDF membranes had improved surface hydrophilicity and higher pure water flux compared with the pristine PVDF membranes.

Hydroxyapatite(HAP) is a promising material due to its good chemical stability and biocompatibility[10-12]. It has been widely used in composite materials including separation membranes. Robinson *et al*.[13] fabricated the hydroxyapatite/polysulfone laminated composites with good biocompatibility and toughness. The toughness and modulus of the composites were close to cortical bone. Fang *et al.*[14] prepared hydroxyapatite whisker-reinforced poly(L-lactic acid) scaffold, which showed high porosity and mechanical strength. Sun fabricated the polyether sulfone(PES)/HAP mixed matrix membranes for protein purification via both diffusion as well as adsorption [15]. Ma *et al.* made Ag-TiO_2/HAP/Al_2O_3 microfiltration membranes with highly reactive photocatalytic for coupling photocatalysis for water treatment, and further investigated the humic acid removal as well as

the anti-fouling properties of membranes[16]. Masmoudi *et al.* obtained a new ceramic asymmetric microfiltration membranes (active layers) based on synthesized lacunary HAP to treat cuttlefish effluents generated from the conditioning seawater products industry, which showed a permeation flux of 125L/h m^2 and a high retention of turbidity (99%), color and COD (92%)[17]. Additionally, HAP whiskers contains abundant hydroxyl groups (-OH) which can improve the hydrophilicity of PVDF membranes. In the previous work[18], the modified PVDF ultrafiltration membranes were successfully prepared by blending method with HAP whiskers. The mechanical properties were significantly improved which can endure long-playing running in industrialized separation field. But the permeation fluxes of PVDF/HAP composite membranes were so low that they might not be suitable for practical applications. According to actuality, it is crucial to prepare practical membranes with high permeation flux, high rejections of solutes as well as good mechanical properties.

Nowadays, many interesting works show that the hydrophilic modifiers can be anchored on membranes by hydrogen bonds. Based on these works and considering the outstanding properties of HAP nano-whiskers with abundant hydroxyl groups, which can form hydrogen bonds with PVP. It can be assumed that the mutual interactions of HAP and PVP contribute to a better dispersion of HAP nano-whiskers. It is crucial to explore the synergetic effects between HAP and PVP in this work. The PVDF/PVP/HAP hollow fiber membranes were synthesized via wet spinning method. The membrane structure and properties were characterized using FESEM, AFM, ATR-FTIR and water contact angle measurements. The ultrafiltration performances were tested by the rejections of three proteins with different molecular weights and humic acid. Furthermore, the crystalline behaviors and mechanical properties were also discussed.

Table 1 The part works about the properties of PVDF membranes modified by inorganic additives

Refs.	Year	Modulus		PVDF membrane	Pure water flux ($L/m^2 \cdot h \cdot bar$)	Rejections (%)/pore size	Contact angle(°)
Zhang[19]	2014	flat sheet	Original	20%PVDF	175	93.8[a]	68
			Modified	3% phosphorylated SNTs	270	95.5[a]	43.2
Hong[20]	2014	flat sheet	Original	17% PVDF	30	30%[b]	70
			Modified	1.5% nano-ZnO	98	98%[b]	63
Zhang[21]	2014	hollow fiber	Original	18%PVDF	80.7	7.0nm[c]	92.6
			Modified	0.75%O-MWNTs	229.4	8.4nm[c]	74.1
Li[22]	2013	flat sheet	Original	19.5% PVDF	36.4	91.6[b]	81
			Modified	1.5% nano-Ag	108.6	88.1[b]	68
Shi[23]	2013	hollow fiber	Original	15% PVDF	190	22.6nm[d]	72.8
			Modified	1% Ag-loaded zeolites	450	25.7nm[d]	78.5
Wei[24]	2011	flat sheet	Original	20%PVDF	80	85[b]	83.3
			Modified	1% TiO_2 nanowires	190	91[b]	35

Yuliwati[25]	2011	hollow fiber	Original	19%PVDF	38	62.6[e] /28.0nm[f]	81.1
			Modified	1.95% TiO_2	90	98.8[e]/34.1nm[f]	47.3
Yu[26]	2009	hollow fiber	Original	18% PVDF	<80	0.074 μm[g]	82.9
			Modified	3% SiO_2	301	0.099μm[g]	53.4
Cao[27]	2006	flat sheet	Original	16%PVDF	88.2	100[b]	78
			Modified	<2% TiO_2	111.7	100[b]	76
Yan[28]	2005	flat sheet	Original	19% PVDF	25	95.5[h]	83.6
			Modified	3% nano-Al_2O_3	125	97.1[h]	58.6
Bae[29]	2005	flat sheet	Original	15% PVDF	303	93[i]	86.7
			Modified	TiO_2/PVDF=0.3	331	95[i]	81.1

a: Rejection of oily wastewater (oil concentration is 45 mg/L); b: Rejection of BSA; c:Pore size determined by solute ultrafiltration; d:Measured by liquid-liquid porometer; e:Rejection of synthetic refinery wastewater; f: Calculated by Guerout-Elford-Ferry equation; g: Mean pore radius determined by filtration velocity method; h: Rejection of PEG Mw=35 000; i: Rejection of PEO with Mw=100 000

2. Experimental

2.1 Materials

PVDF(FR904) in powder form was purchased from Shanghai 3F New Material Co. Ltd. (China). Polyvinylpyrrolidone (PVP K30) were purchased from Shanghai Aladdin Chemical Agent Co. Ltd. (China). N-methyl-2-pyrrolidone(NMP) involved as solvent was purchased from Sino-pharm Chemical Reagent Shanghai Co. Ltd.(China). Lysozyme (M_W=14 400), albumin (M_W=45 000) and bovine serum albumin (BSA, M_W=6 7000) were purchased from Shanghai Bio Co. Ltd (China). Humic acid (fulvic acid content>90%) was purchased from Shanghai Aladdin Chemical Agent Co. Ltd. (China). Deionized water (DI) was self-produced by a reverse osmosis (RO) system. All other chemicals were purchased from Sino-pharm Chemical Reagent Shanghai Co. Ltd. (China).

HAP nano whiskers were self-synthesized by wet chemical precipitation method, which was described in the previous work[18]. The nano whiskers have a mean length HAP of 116.2±8.5 nm, and average width of 20.8±3.5nm according to the TEM images.

2.2 Light transmittance measurements of dope solutions

The precipitation kinetics of PVDF/PVP/HAP dope solutions were measured by light transmittance measurements. The detailed experimental procedure and the schematic of equipment were described in the previous works[30, 31]. The cast pristine film was immersed into coagulation bath(tap water) at 25 $^{\circ}$C. The intensity of the transmitted light through cast film in water bath was measured in terms of time. The signal of the transmitted light was detected and recorded by a computer, indicating the precipitation rate of dope.

2.3 Dope rheology measurements

The rheology properties of the PVDF/PVP/HAP dopes were measured by a rotational rheometer

(Austria Anton Paar MCR102) with a parallel of plate geometry at 25 °C. The samples were placed between the parallel plates. The shear rate ranged from 0.001s^{-1} to 1000 s^{-1}.

2.4 Membrane preparation

The dope solutions for membrane spinning contained quantified PVDF, PVP and different amounts of HAP(1.0-3.0 wt.%). The residuals were balanced with NMP solvent. The mixtures were stirred for 12 h at 60 °C to obtain homogeneous dope solutions. The dopes were degassed for 12 h before spinning.

The hollow fiber membranes were spun at 25±1 °C with wet spinning method. The dope solution and bore fluid passed through a spinneret with an orifice diameter/inner diameter of 0.9/0.5 mm at the pressure of N_2 and constant-flow pump, respectively. The bore fluid was 90 wt.% NMP aqueous solution. Outer coagulation liquid was tap water at 25±1°C. The ratio of dope flow rate to bore fluid flow rate was constant in all spinning processes. The fabricated fibers were stored in deionized water bath for 24 h to remove any residual solvent. Then, the fibers were kept in 50 wt.% glycerol aqueous solution for 24 h to avoid the collapse of porous structure and stored in a sealed space at room temperature for testing. The detailed preparation conditions and geometrical parameters of PVDF/PVP/HAP hollow fiber membranes were listed in Table 2 and Table 3, respectively.

Table 2 The detailed preparation conditions of PVDF/PVP/HAP hollow fiber membranes

Membrane no.	Composition of dope solution(%) PVDF/HAP/PVP/NMP	Bore fluid
M-1	18/0/3/79	NMP/H_2O:90/10
M-2	18/1/3/78	NMP/H_2O:90/10
M-3	18/2/3/77	NMP/H_2O:90/10

M-4	18/3/3/76	NMP/H_2O:90/10
M-5	18/1/0/81	NMP/H_2O:90/10

Table 3 The geometrical parameters of PVDF/PVP/HAP hollow fiber membranes

Membrane no.	OD(mm）	ID(mm)	δ(mm)	CA(°)	ε(%)	r_m(nm)
M-1	1.150	0.635	0.258	89.2±2.7	79.4	14.7
M-2	1.025	0.515	0.255	83.3±3.6	78.7	23.1
M-3	0.990	0.555	0.218	75.2±2.1	77.4	19.3
M-4	1.035	0.635	0.205	68.3±2.9	76.9	16.1
M-5	1.015	0.610	0.203	91.4±2.5	76.4	5.8

Note: OD-outer diameter, ID-inner diameter, δ-wall thickness, CA-final contact angle, ε -porosity, r_m-mean pore radius.

2.5 Membrane characterizations

2.5.1 Morphologies of PVDF/PVP/HAP hollow fiber membranes

The morphologies of PVDF/PVP/HAP hollow fiber membranes were examined by a field emission scanning electronmicroscopy (FESEM) (Hitachi S-4800). The hollow fiber membranes were firstly immersed in absolute ethanol for about 10 min, and then fractured in liquid nitrogen to obtain clear cross-sections. Then the samples were positioned on a metal holder and gold coated under vacuum. The FESEM images of the outer surfaces, inner surfaces and cross-sections of hollow fiber membranes were collected. In order to insight the dispersion of HAP nano-whiskers in the membranes, the map scan spectra of energy dispersion of X-ray(EDX) were conducted on the external surfaces of the PVDF/PVP/HAP hollow fiber membranes.

The outer surfaces of the fabricated PVDF/PVP/HAP hollow fiber membranes were also detected by an atomic-force microscopy (AFM, BioScope TM, USA) using tapping mode. Small squares of the prepared membranes were placed in a glass substrate and the surface was imaged at a scan size of 2μm×2μm. Scanning was performed at a speed of 2 Hz. The mean roughness (R_a) is the average value of the surface relative to the center plane for which the volumes enclosed by the image above and below the plane are equal. Each sample was measured for 3 times at different points on the outer surface so that the data were much more convincing.

2.5.2 Hydrophilicity, porosity and pore size measurements

The surface hydrophilicity was evaluated by dynamic contact angle, which was conducted on a contact angle analyzer (KRUSS DSA30 German). The measurements on the outer surfaces of membranes were carried out using a droplet of 3.0 μL at room temperature. All tests were recorded in movies for 10 min and repeated for at least 3 times to minimize experimental error. The membrane porosity ε **(%)** was defined using gravimetric method, as defined in the following equation

$$\varepsilon(\%) = \frac{w_1 - w_2}{V_{membrane} \times d_w} \times 100\% \qquad \text{Eq.(1)}$$

$$V_{membrane} = \frac{\pi}{4} \times (\mathrm{d}_{OD}{}^2 - \mathrm{d}_{ID}{}^2) \times L \qquad \text{Eq.(2)}$$

where w_1 and w_2 was the weight of wet and dry membranes(g), respectively. The value of d_w was the pure water density(0.998g/cm^3), $V_{memrbane}$ was the volume of hollow fiber membrane(m^3), which could be calculated by Eq.(2), where d_{OD} and d_{ID} represent the outer diameter and inner diameter of hollow fiber membrane, respectively and L was the length of membranes[32].

In addition, in order to determine the membrane mean pore radius($\boldsymbol{r_m}$), Guerout-Elford-Ferry equation on the basis of the pure water flux and porosity data was used[32, 33],

$$r_m = \sqrt{\frac{(2.9-1.75\varepsilon)8\eta l Q}{\varepsilon \times A \times \Delta P}} \quad \text{Eq.(3)}$$

where η is the water viscosity(8.9×10^{-4}Pa s), Q is the volume of permeate water per unit time(m^3/s), and ΔP is the operation pressure(0.1MPa).

2.5.3 Permeation and rejection performances of PVDF/PVP/HAP hollow fiber membranes

The permeation and rejections of the PVDF/PVP/HAP hollow fiber membranes were measured by ultrafiltration experiments. Three different protein aqueous solutions of lysozyme (M_W=14 400), albumin (M_W=45 000) and bovine serum albumin (BSA, M_W=6 7000) were applied to solute transport experiments. The feed concentrations of protein aqueous solutions (pH=7) were kept at 500 ppm. The humic acid(HA) with the concentration of 50 ppm also measured. Hollow fiber membrane modules were self-prepared (outside feeding) which were detailedly described in the previous works[30, 34, 35]. All experiments were conducted at 25±1 °C with a feed pressure of 1.0 bar. The newly prepared membranes were pre-pressured at 2.0 bar with deionized water for 1 h before measuring. After that the pure water permeability (PWP, J_w) being tested, the measurements of the permeation and rejections for protein and HA aqueous solutions were followed. The proteins and HA concentrations of both feed and permeate solutions were determined by an ultraviolet spectrophotometer (UV3600 Shimadzu, Japan). The J_w and rejection (R) were defined as formulas (4) and (5), respectively

$$J_w = \frac{Q}{\Delta P \times A} \quad \text{Eq.(4)}$$

$$R = (1-\frac{A_i}{A_0})\times 100\% \quad \text{Eq.(5)}$$

where Q was the volumetric flow rate ($L\cdot H^{-1}$), ΔP was the transmembrane pressure (bar), A was the effective membrane area, R was the rejection for proteins, A_i and A_0 were the absorption value of the permeate solution and feed solution, respectively.

After the permeation experiments with BSA aqueous solution, the fouled membranes (M-2) were immediately washed for 30 min with a 500ppm NaClO aqueous solution at 25 °C. After washing, the membrane module was rinsed with DI water, and then the *PWP* value was tested again. It was conducted with thrice fouling and twice washing. The flux recovery ratio (FRR) was evaluated by[11]

$$FRR(\%) = J_R / J_W \times 100 \quad \text{Eq. (6)}$$

where J_R is re-measured PWFs of the membranes in each cycle.

2.5.4 ATR-FTIR and XRD of PVDF/PVP/HAP hollow fiber membranes

The attenuated total reflectance Fourier transform infrared (ATR-FTIR) spectra of PVDF/PVP/HAP hollow fiber membranes were collected with a Nicolet 380 (Thermo Electron Corporation, USA) spectrometer with a resolution of 4 cm^{-1} in the wavenumber of 400-4000 cm^{-1}. The crystalline behaviors of the samples were detected by a wide-angle X-ray diffraction (WAXD, D/max-II B, Japan) in the 2θ range of 5-50°.

2.5.5 Mechanical properties

The mechanical properties of PVDF/PVP/HAP hollow fiber membranes were tested according to Chinese National Standard(GB/T228-2002). It was tested by a material test machine (QJ210A, Shanghai Qingji Instrumentation Sci. & Tech. Co., Ltd, Shanghai, China). The loading velocity is 50 $mm \cdot min^{-1}$. The presented values were obtained by measuring at least five times for each sample and then averaged.

3. Results and discussion

3.1 Rheology properties and precipitation kinetics of PVDF/PVP/HAP dope solutions

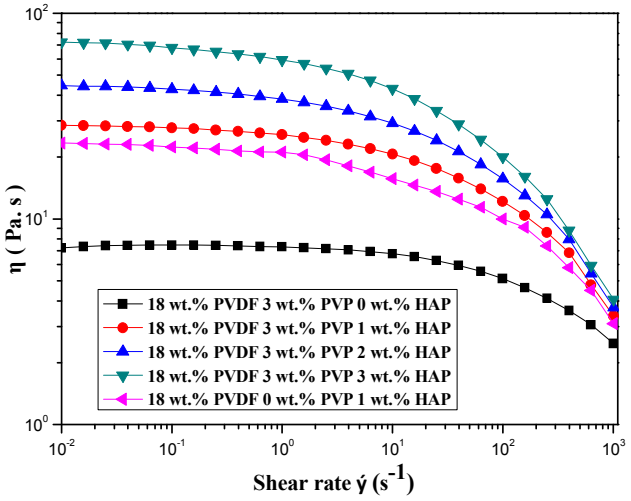

Fig.1 The viscosity versus shear rate of PVDF/PVP/HAP dopes

Fig.1 shows the shear viscosity versus shear rate of five dopes. A Newtonian behavior at lower shear rate and a shear-thinning behavior at higher shear rate are observed [36]. The interactions between PVDF chains and HAP whiskers are enhanced with the increase of HAP loading. Therefore, the addition of HAP restrains shear flow of dope and results in an increase of viscosity[37]. Moreover, the viscosity presents a sharp decline in the shear rate of 10-10^3 s^{-1} for the five samples. It is the result of weak flow-impeding effect at higher shear rate for polymer chains[38]. The interactions between PVDF chains and HAP whiskers are weaker than Van der Waals force in the chain coins so that it is easily destroyed preferentially to the disentanglement of chain coins in shear flow. This phenomenon contributes to the more significant shear thinning behavior of the dope[37]. The dope only containing 1wt.% HAP shows lower viscosity than that of dope containing dual additives(3wt.% PVP and 1wt.% HAP). The abrupt viscosity drop is probably due to interfacial slip between the PVDF and HAP whiskers without PVP, implying that PVP actually improves the compatibility between HAP and PVDF. As a consequence, the addition of HAP whiskers can increase the viscosities of dopes, which

subsequently affects the precipitation kinetics and structure of the resultant membranes.

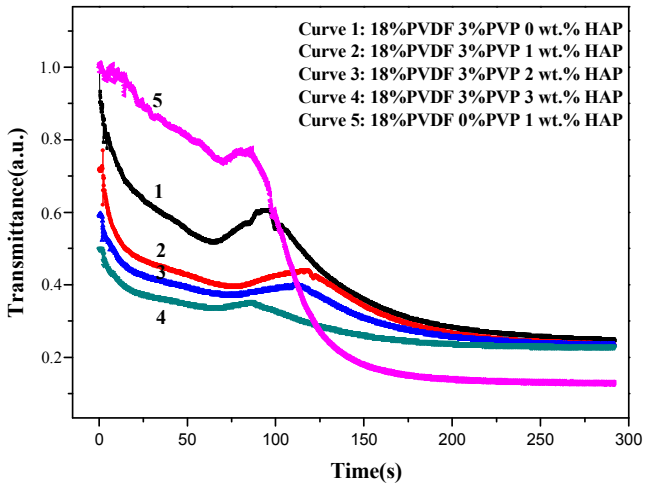

Fig.2 Effect of HAP content on the precipitation kinetics of PVDF/PVP/HAP dope solutions

To examine the precipitation kinetics of PVDF/PVP/HAP dopes, the light transmittance measurements are performed and plotted in Fig.2. It can be easily observed that the five dopes exhibit instantaneous demixing phenomena. Because the PVP and HAP nano whiskers are hydrophilic substances which can accelerate the mutual mass transfer between solvent and non-solvent, and lead to high precipitation rate. Furthermore, the precipitation rate decreases with the increasing addition of HAP whiskers, which can be demonstrated from the decreasing gradient of the four curves. The phenomenon may be caused by the effects of HAP whiskers on solution viscosity[39]. The increasing viscosity of dope solution restrains the diffusions of solvent and non-solvent in the precipitation process and affects the demixing rate. The curve 5 in Fig.2 shows that the dope containing 1wt.% HAP without PVP shows the lowest demixing rate in the initial 70 seconds. Moreover, there's a peak in each curve which also can be seen in the previous work[31]. The peaks should be attributed to the re-dissolution of the dense skin layer by solvent, which is inhibited by the just-formed skin layer. The

region below skin layer presents high solvent concentration which dissolves it and leads to the increase of light transmittance.

3.2 Morphologies of PVDF/PVP/HAP hollow fiber membranes

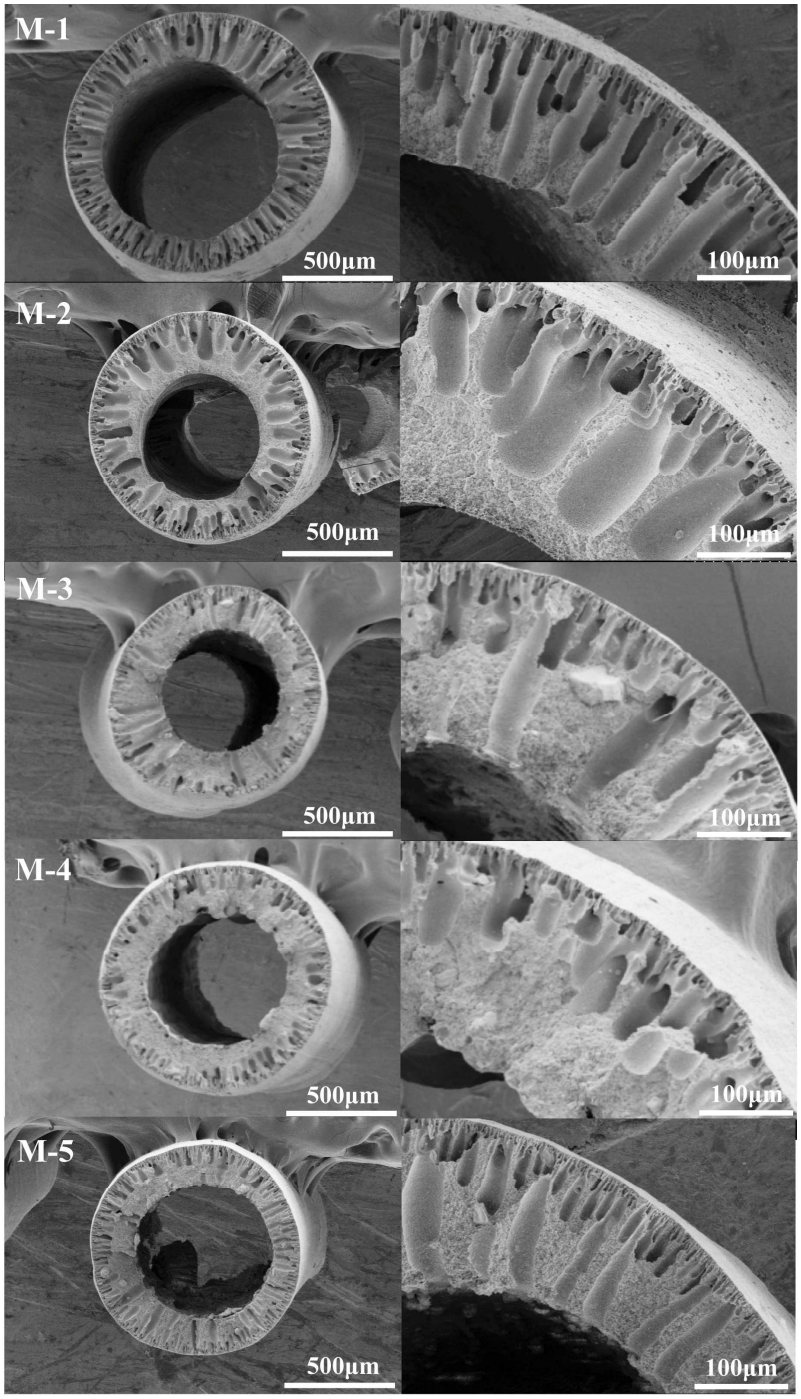

Fig.3 FESEM images of the cross-sectional morphologies of PVDF/PVP/HAP hollow fiber membranes

From Fig.3, the cross sections of PVDF/PVP/HAP hollow fiber membranes present the asymmetric structure which consists of a dense top layer and a porous sub-layer, respectively. Without the addition of HAP, the finger-like pores run through the whole cross-section of membrane for M-1. It can be explained that water acting as a strong non-solvent gives a higher precipitation rate, which leads to a higher growth rate of finger-like pores; while 90 wt.% NMP aqueous solution almost cannot induce the demixing of dopes. As a result, the finger-like pores can extend straightly to the inner surface of M-1. When 1wt.% HAP whisker is added, the finger-like pores become shorter and wider for M-2 compared to M-1. With the further addition of 2 wt.% and 3 wt.% HAP whisker, the finger-like pores are significantly suppressed and further replaced by sponge-like structure. The finger-like structures presented in PVDF/PVP/HAP hollow fiber membranes are the typical results of the instantaneous demixing of dopes, which is illustrated in Fig.2. However, with the addition of HAP, the increased viscosity of dopes (Fig.1) restrains the growth of finger-like pores. Additionally, the increased viscosity enhances the ratio of non-solvent inflow to solvent outflow, which results in the appearance of sponge-like structure in the inner layers[40]. Compared to M-2, the membrane of M-5 containing single HAP additive exhibits narrower finger-like pores due to the absence of PVP.

Fig.4 and Fig.5 illustrate the morphologies of the outer surfaces and inner surfaces of PVDF/PVP/HAP hollow fiber membranes. It can be observed that the outer surfaces are dense because the strong non-solvent(water) is used as the outer coagulation liquid. From Fig.5, the membranes of M-1~M-5 exhibit the porous inner surfaces because 90wt.% NMP aqueous solution is involved as bore liquid.

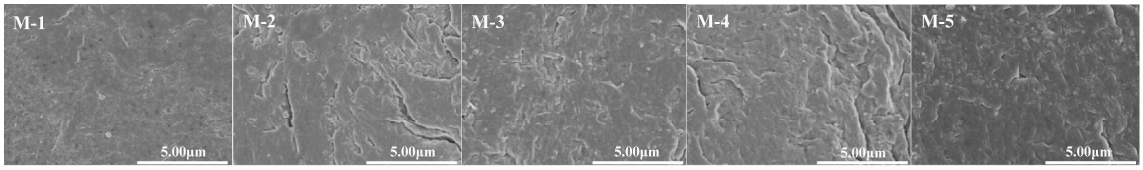

Fig.4 FESEM images of the outer surfaces of PVDF/PVP/HAP hollow fiber membranes

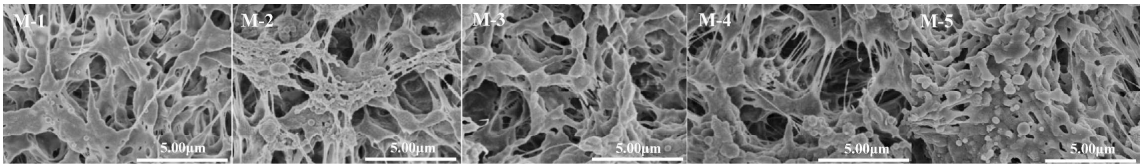

Fig.5 FESEM images of the inner surfaces of PVDF/PVP/HAP hollow fiber membranes

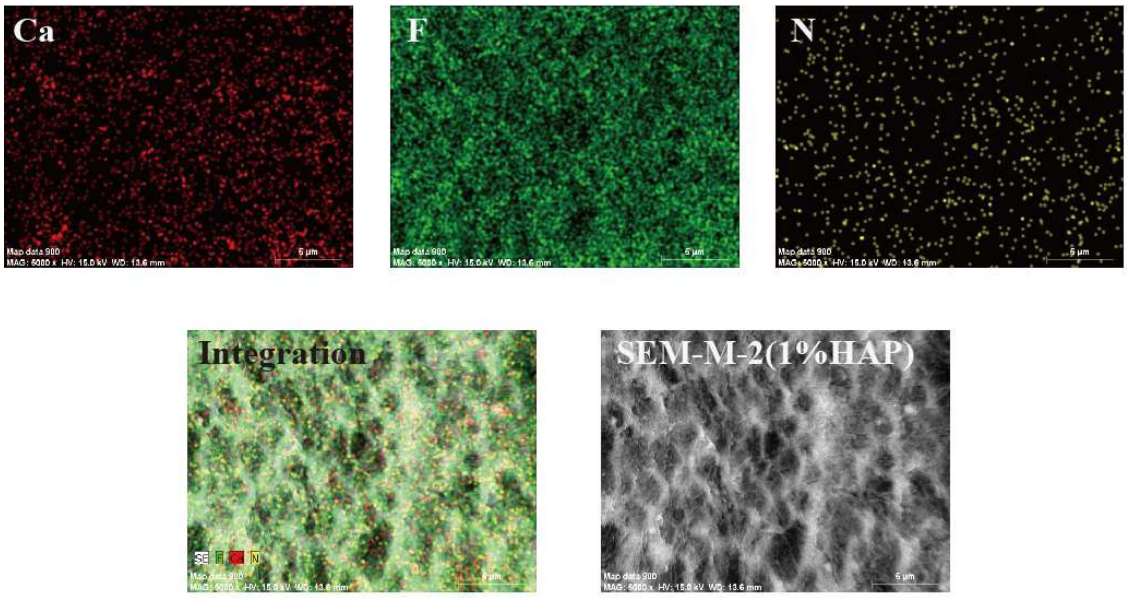

Fig.6 EDX map scanning spectra for the outer surface of M-2

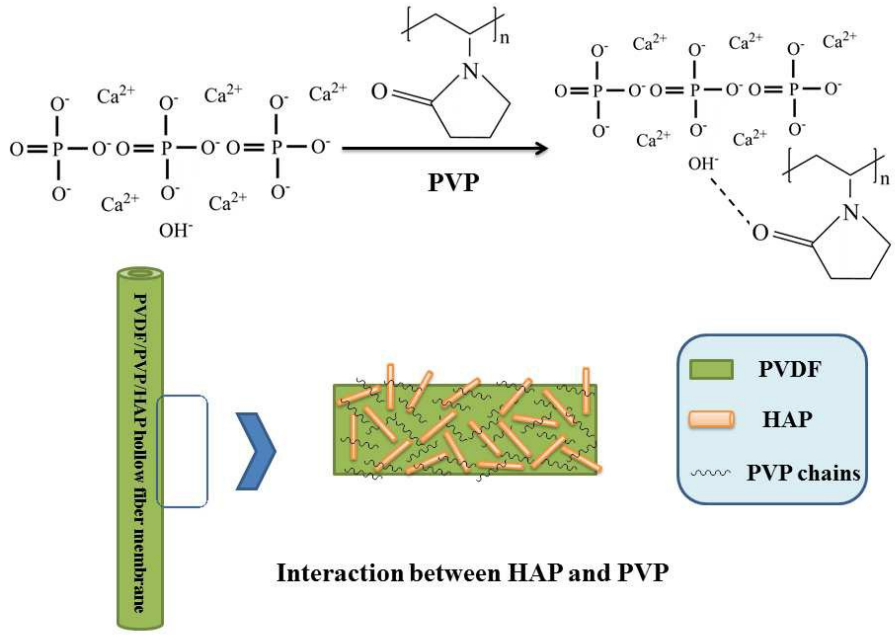

Fig.7 The brief illustration of the interactions between PVP and HAP

The EDX map spectra of M-2 in Fig.6 show the dispersion of HAP and PVP in membrane. The red, green and yellow spots in Fig.6 corresponding to calcium(Ca), fluorin(F) and nitrogen(N) represent HAP, PVDF and PVP components, respectively. The EDX map spectra present the uniform distribution of calcium, which indicates the good dispersion of HAP in PVDF/PVP/HAP hollow fiber membranes. The graphical representation in Fig.7 illustrates that HAP nano-whiskers and PVP have good interactions via hydrogen bonds, which contributes to the good dispersion of HAP and properties of the resultant membranes.

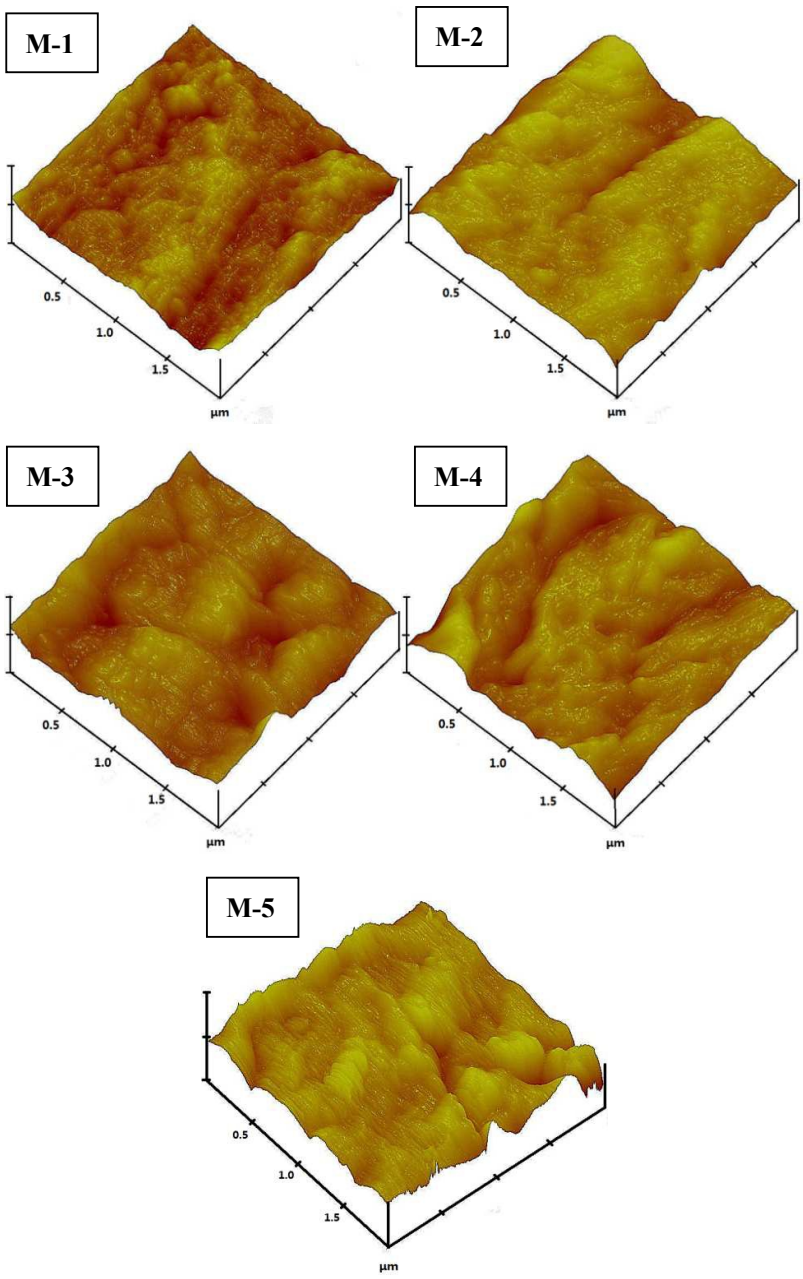

Fig.8 AFM images of the outer surfaces of PVDF/PVP/HAP hollow fiber membranes

The outer surfaces of M-1~M-5 are also detected by AFM technique with tapping mode. The images and roughness parameters are illustrated in Fig.8 and Table 4. The average roughness(R_a), root-mean-square(RMS) roughness(R_q), surface skewness(R_{sk}) and surface kurtosis(R_{ku}) are chosen to analyze the surface roughness. Table 4 presents the roughness parameters, which clearly show a trend

highly related to HAP content in the dope solutions. It can be easily observed that M-1 without the addition of HAP is smoother than others. With the addition of HAP, the surface becomes rougher. The R_a and R_q evidently increase as HAP content increases from 0 wt.% to 2 wt.% for M-1~M-3. It may be caused by the accelerated solidification rate with HAP addition, which restrains the relaxation of orientated macromolecules to return original state[35]. As the addition of HAP increases up to 3 wt.%, the R_a and R_q vary little. It can be explained that the increasing viscosity of dope solution slows the solidification rate. The membrane of M-5 with single HAP, which shows lower surface roughness compared to M-2. It may closely relate to the lacking of PVP, which decrease the dope viscosity. The value of surface skewness(R_{sk}) is 0.122 of M-1, implying that the surface comprises peaks rather than cavities of M-1. With the addition of HAP, the negative values demonstrate the dominance of valleys. The R_{ku} below 3 for M-1 implies that it has a flat and repetitive surface. On the contrary, the values of M-2~M-4 are more than 3 which suggest sharp height distributions in comparison with M-1.

Table 4 The quantitative summary of the surface roughness of M-1~M-5

Membrane no.	R_a(nm)	R_q(nm)	R_{sk}	R_{ku}
M-1	7.214	8.678	0.122	2.647
M-2	15.245	18.066	-0.534	3.984
M-3	21.438	26.765	-0.329	3.296
M-4	21.259	26.517	-0.104	3.292
M-5	9.759	12.207	0.105	3.416

3.3 Hydrophilicity, porosity and pore size measurements

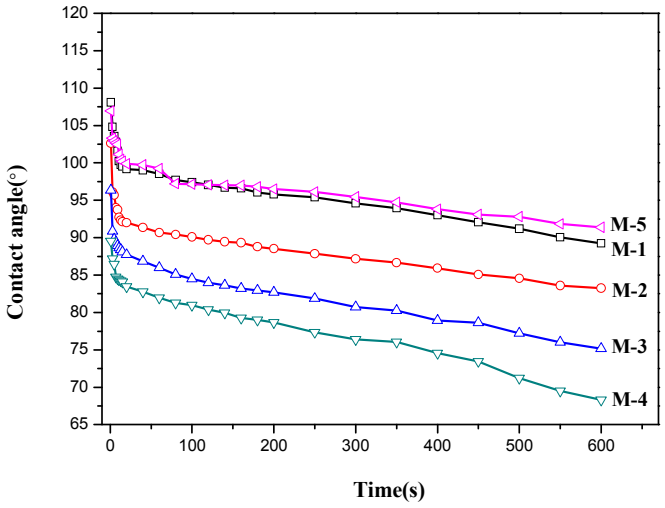

Fig.9 The dynamic contact angles of PVDF/PVP/HAP hollow fiber membranes

Dynamic contact angle is widely used for the characterization of surface hydrophilicity of membranes. Surface hydrophilicity is one of the most important factors, which could affect the permeation flux and antifouling ability of membranes[41]. The dynamic contact angles of PVDF/PVP/HAP hollow fiber membranes are illustrated in Fig.9, and the final values are collected in Table 3. From Fig.9 and Table 3, it can be easily observed that the contact angle decreases as the content of HAP whiskers increases from 0 wt.% to 1 wt.%, 2 wt.% and 3 wt.% for the membranes of M-1~M-4. After incorporation of hydrophilic HAP whiskers, the water contact angles of PVDF/PVP/HAP hollow fiber membranes decrease as the HAP content increases. The membranes of M-1 and M-5 containing a single additive(PVP or HAP) show similar contact angles, which are clearly higher than those of the membranes(M-2~M-4) containing dual additives. It verifies that PVP and HAP additives have synergistic effects in improving the surface hydrophilicity. It should be advantageous to the improvement of water permeation and antifouling ability of the resultant membranes.

It can be seen from Table 3, the porosity(ε) of M-2~M-4 slightly decreases with the increase of HAP loading in membranes, which is consistent to the morphologies shown in Fig.3. From Table 3, compared with M-1, the mean pore radius (r_m) firstly increase with the addition of 1.0 wt% HAP for M-2, and then decrease with the further addition of HAP whiskers for M-3 and M-4. The membrane of M-5 containing only single additive HAP has the smallest r_m of 5.8 nm. This phenomenon is consistent with the membrane morphologies.

3.4 Hydraulic permeability and rejections of PVDF/PVP/HAP hollow fiber membranes

Table 5 summaries the permeation fluxes and rejections of PVDF/PVP/HAP hollow fiber membranes. As shown in Table 5, for the membranes of M-1~M-4, the pure water permeation flux first increases with the addition of HAP and attains the peak value when HAP content is 1 wt.%. With the further addition of HAP, the J_w value of PVDF/PVP/HAP hollow fiber membranes decreases from 549.1 $L \cdot M^{-2} \cdot H^{-1} \cdot bar^{-1}$ for M-2 to 425.9 and 316.3 $L \cdot M^{-2} \cdot H^{-1} \cdot bar^{-1}$ for M-3 and M-4 respectively. It is generally accepted that the water permeation flux J_w is mainly determined by the morphology and surface hydrophilicity of membranes. The increase of J_w from 224.2 to 549.1 $L \cdot M^{-2} \cdot H^{-1} \cdot bar^{-1}$ can be ascribed to the improved hydrophilicity of membrane surface by adding HAP nano whiskers (Fig.9 and Table 3). The membrane of M-5 only containing HAP presents the smallest J_w value due to the absence of PVP as porogen. The rejections of lysozyme, albumin, BSA and HA also detailedly listed in Table 5. It shows that the higher rejections of BSA and HA than those of other two solutes are obtained. From Table 3, it also can be seen that the rejections of solutes decrease with the increase of HAP content in the membranes of M-1~M-4. The membrane of M-5 exhibits much higher rejections of solutes in the membranes except for M-1. The membrane of M-2 exhibits the highest pure water flux accompanied with 89.4% rejection of BSA and 82.9% rejection of HA. These results prove that

the prepared PVDF/PVP/HAP hollow fiber membranes owning ultrafiltration performance. By comparing M-2 and M-5, it can be seen that the introducing of PVP increases the water permeability more than 12 times by decreasing the rejection of proteins a little. This is attributed to the addition of PVP and synergism with HAP, which play an important role in improving PVDF hollow fiber membranes. The experimental results indicate that the membranes with single additive (HAP or PVP) cannot present satisfied hydrophilicity and permeation performances.

Table 5 Permeation and rejections of PVDF/PVP/HAP membranes

Membrane	J_w	*FRR*	Rejections			
no.	($L \cdot M^{-2} \cdot H^{-1} \cdot bar^{-1}$)	(%)	Lysozyme	Albumin	BSA	HA
M-1	224.2±6.9	54.7	81.5%	84.9%	98.4%	92.7%
M-2	549.1±12.2	56.5	50.6%	77.2%	89.4%	82.9%
M-3	425.9±16.2	68.6	50.2%	68.3%	87.2%	81.5%
M-4	316.3±18.9	70.5	36.4%	49.1%	80.5%	72.9%
M-5	41.47±4.1	61.4	67.2%	79.7%	97.8%	89.4%

3.5 Flux decay and regeneration of PVDF/PVP/HAP hollow fiber membranes

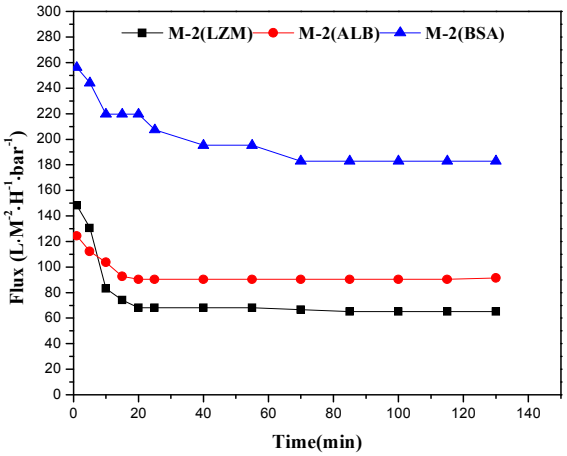

Fig.10 Permeation flux for different protein solutions in terms of running time

A satisfied membrane should has low fouling tendency accompanied with high flux and rejection over a long operating time[32]. In the ultrafiltration of BSA solution, M-2 exhibits the maximum permeation flux. It is chosen to measure the permeation fluxes for lysozyme, albumin and BSA solutions as a function of running time. The permeation flux profiles as a function of running time for lysozyme, albumin and BSA are depicted in Fig.10. The results indicate that M-2 exhibits the lowest stable permeation flux for lysozyme (14.4 kDa) solution, the highest one for BSA(67 kDa) solution and a medium one for albumin(45 kDa) solution. This phenomenon suggests that the molecular-weight of protein is highly related with the stable permeation flux for membranes. It should be explained that the protein with low molecular weight easily enters into membrane pores and results in a low permeation flux [42, 43].

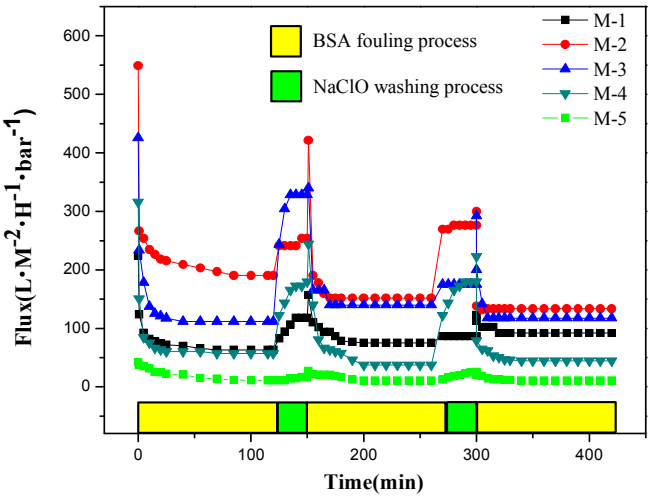

Fig.11 Time-dependent flux of PVDF/PVP/HAP hollow fiber membranes with 3 ultrafiltration and cleaning cycles

To investigate the effects of HAP nano whiskers on fouling resistance, the cyclic ultrafiltration measurements are performed on the membranes of M-1~M-5 and illustrated in Fig.11. The

ultrafiltration process can be divided into 3 steps. The membranes are firstly fouled by the ultrafiltration of 500 ppm BSA aqueous solution for 130 min. Then the fouled membranes are washed with 500 ppm NaClO solution. The pure water fluxes of the membranes are measured again after 30min washing. The permeation flux profiles are plotted in Fig.11.

From Fig.11, it can be seen that all membranes have a slightly decline in permeation flux and hydraulic permeability after 3 cycles. The flux decline is mostly caused by the irreversible membrane fouling which might be entrapped in the outer surface as well as in the pores[44]. The loss of PVP after washed by NaClO may be also one reason, which has been revealed in the previous work[45]. It leads to the decline of surface hydrophilicity of membranes and make the resultant membranes be easily fouled by BSA protein. The higher operating fluxes with BSA solution of M-1 and M-3, which can be considered as the change in the morphology after the repeated NaClO cleaning process. The loss of PVP destroys the membrane skin layer to a certain degree, which may enlarge the pore size and lead to the small rise of flux.

From Table 5, it also can be seen that FRR gradually increase from 54.7% to 70.5% with the addition of HAP in the membranes of M-1~M-4, implying the introduced HAP whiskers contribute to the permeation flux recovery of the fouled membrane. For the membrane of M-5 containing single HAP also has a medium FRR of 61.4%.

3.6 Crystallization behaviors of PVDF/PVP/HAP membranes by ATR-FTIR and XRD

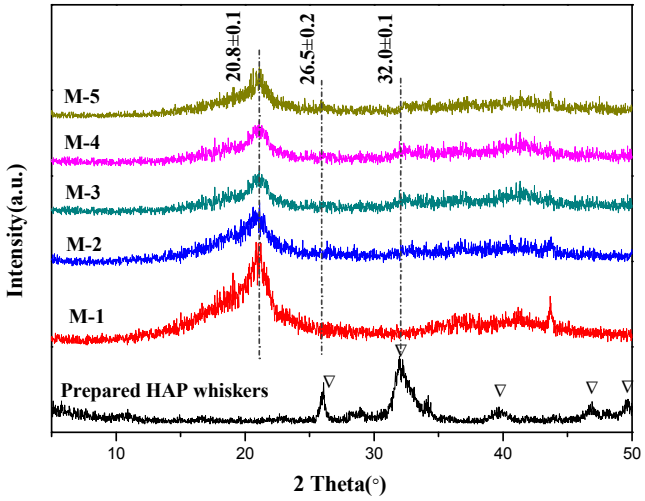

Fig.12 XRD patterns of PVDF/PVP/HAP hollow fiber membranes and HAP whiskers

PVDF is semi-crystalline polymer which exhibits at least four crystalline forms, i.e. α-, β-, γ-, and δ-phases[46]. To further investigate the crystallization behaviors of PVDF in the membranes, XRD and ATR-FTIR measurements are carried out to detect the PVDF crystalline phases. Fig.12 shows the XRD patterns of the PVDF/PVP/HAP hollow fiber membranes and HAP whiskers. The XRD curves and characteristic peaks of HAP whiskers are clearly illustrated in Fig.12, implying that the HAP whiskers are prepared with perfect crystallization[47]. A sharp peak at 20.8˚ can be assigned to the (110) and (200) reflections of β-phase of PVDF for all membranes[46]. With the addition of HAP, the weak diffraction peaks at 26˚ and 32.0˚ can be detected for the membranes, especially for M-3 and M-4, implying that the existence of HAP whiskers in the resultant membranes in accordance with the characteristic peak of HAP whiskers.

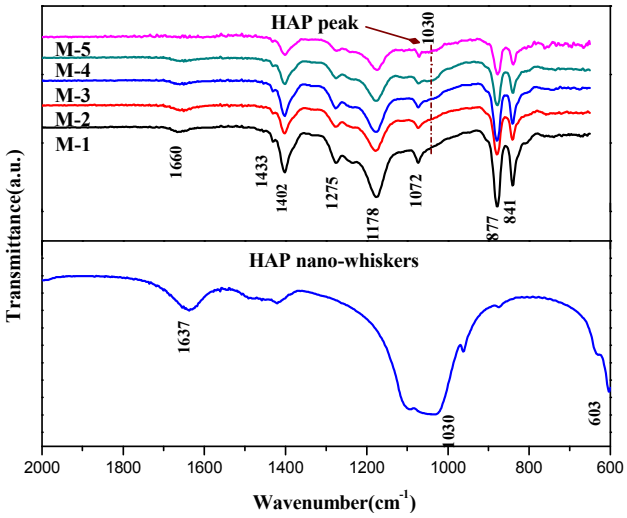

Fig.13 FTIR spectra of PVDF/PVP/HAP hollow fiber membranes and HAP nano-whiskers

The ATR-FTIR spectra can further verify the crystalline structure of PVDF/PVP/HAP hollow fiber membranes (Fig.13). The intensive peaks at 1660 cm^{-1} can be assigned to the stretching vibration of the C=O bond in PVP[48]. The characteristic peaks of β-phase crystallite structure at 841, 877, 1178, 1275, 1402 and 1433 cm^{-1} are shown in all membranes[18, 49]. The increasing intensity at 1030 cm^{-1} for M-2~M-5 demonstrates the existence of HAP whiskers in membrane matrix[50].

3.7 Mechanical properties of PVDF/PVP/HAP hollow fiber membranes

Table 6 Mechanical properties of PVDF/PVP/HAP hollow fiber membranes

Membrane no.	Tensile strength (MPa)	Elongation at break (%)	Young modulus (MPa)
M-1	1.9±0.1	55.5±3.8	32.5±3.2
M-2	2.7±0.1	70.8±4.9	41.7±5.6
M-3	3.0±0.2	72.1±5.0	61.7±4.9
M-4	3.5±0.2	76.3±7.8	46.1±2.7
M-5	2.6±0.2	44.7±5.7	61.2±4.9

The mechanical properties of PVDF/PVP/HAP hollow fiber membranes in terms of tensile strength, elongation at break and Young's modulus are shown in Table 6. With the addition of HAP whiskers in dope solution, the corresponding membranes present the improved mechanical properties. The tensile strength and elongation at breaking increase from 1.9 MPa, 55.5% for M-1 to 3.5 MPa, 76.3% for M-4 respectively. The Young modulus also increases from 32.5 MPa for M-1 to 61.7 for M-3, and then decreases to 46.1 MPa for M-4. The fiber of M-5 with single HAP additive has the similar tensile strength to that of M-2, a lower elongation ratio and a higher Young modulus than that of M-2, which can be ascribed to the structure difference of them. The enhanced mechanical properties of PVDF/PVP/HAP membranes should be ascribed to the inherent mechanical strength of HAP whiskers as well as the good interactions between HAP nano whiskers and PVDF/PVP chains. The reinforcing behaviors for polymers with HAP whiskers were also extensively investigated in many other composite materials [51-53].

4. Conclusion

The PVDF/PVP/HAP hollow fiber membranes were fabricated via wet spinning method with 90wt.% NMP aqueous solution as bore liquid. The morphologies, surface hydrophilicity, permeation performances and mechanical properties of the fabricated membranes as well as the properties of dopes were well characterized by numerous state-of-the-art analytical techniques. The results verify that HAP content and bore liquid evidently influence the morphologies and properties of the resultant membranes. With the addition of HAP, the finger-like structure is gradually suppressed and replaced by sponge-like structure, and the surface hydrophilicity is evidently improved. The outer surface becomes rougher after adding HAP in the membranes. As 90wt.% NMP aqueous solution is used as bore liquid, the hydraulic permeability J_W of the membranes(M-1~M-4) firstly increases from 224.2 of

M-1 to 549.1 $L \cdot M^{-2} \cdot H^{-1} \cdot bar^{-1}$ by adding 1.0 wt.% HAP nano whiskers in the dope, and then decreases to 425.9 and 316.3 $L \cdot M^{-2} \cdot H^{-1} \cdot bar^{-1}$ with the further addition to 2wt.% and 3wt.% in the dopes. The rejections of three proteins and humic acid slightly decrease as HAP content increases in the membranes. The fibers are evidently reinforced, and the three mechanical indicators are gradually improved with the addition of HAP whiskers in the membranes.

Acknowledgments

The research is supported by Science and Technology Commission of Shanghai Municipality (13ZR1429900, 14520502900) and Internation Joint Laboratory on Resource Chemistry (IJLRC).

Nomenclature

OD-outer diameter (mm)

ID-inner diameter (mm)

δ -wall thickness (mm)

CA-contact angle

ε -porosity(%)

r_m-mean pore radius (nm)

J_w-hydraulic permeability ($L \cdot M^{-2} \cdot H^{-1} \cdot bar^{-1}$)

Q-the volumetric flow rate ($L \cdot H^{-1}$)

ΔP-the transmembrane pressure (bar/Pa)

A-the effective membrane area (m^{-2})

R-the rejection for PEG solute (%)

A_i-absorption value of the permeate solution and feed solution

A_0-absorption value of the feed solution

FRR-flux recovery ratio (%)

C_P-the concentrations of permeate (g/L)

C_F-the concentrations of feed solutions (g/L)

X_C-the crystallinity of sample(%)

R_a-the mean roughness of the membrane surface (nm)

R_q-the root-mean-square roughness(nm)

η-the viscosity of dope solution(Pa·s)

References

[1] F. Liu, N.A. Hashim, Y. Liu, M.R.M. Abed, K. Li, Progress in the production and modification of PVDF membranes, J. Membr. Sci., 375 (2011) 1-27.

[2] G.-d. Kang, Y.-m. Cao, Application and modification of poly(vinylidene fluoride) (PVDF) membranes – A review, J. Membr. Sci., 463 (2014) 145-165.

[3] M.-m. Tao, F. Liu, B.-r. Ma, L.-x. Xue, Effect of solvent power on PVDF membrane polymorphism during phase inversion, Desalination, 316 (2013) 137-145.

[4] Y. Shen, A.C. Lua, Preparation and characterization of mixed matrix membranes based on PVDF and three inorganic fillers (fumed nonporous silica, zeolite 4A and mesoporous MCM-41) for gas separation, Chem. Eng. J., 192 (2012) 201-210.

[5] Z. Yuan, X. Dan-Li, Porous PVDF/TPU blends asymmetric hollow fiber membranes prepared with the use of hydrophilic additive PVP (K30), Desalination, 223 (2008) 438-447.

[6] S. Boributh, A. Chanachai, R. Jiraratananon, Modification of PVDF membrane by chitosan solution for reducing protein fouling, J. Membr. Sci., 342 (2009) 97-104.

[7] M. Zhang, Q.T. Nguyen, Z. Ping, Hydrophilic modification of poly (vinylidene fluoride)

microporous membrane, J. Membr. Sci., 327 (2009) 78-86.

[8] C.Y. Lai, A. Groth, S. Gray, M. Duke, Enhanced abrasion resistant PVDF/nanoclay hollow fibre composite membranes for water treatment, J. Membr. Sci., 449 (2014) 146-157.

[9] C.H. Loh, R. Wang, Effects of Additives and Coagulant Temperature on Fabrication of High Performance PVDF/Pluronic F127 Blend Hollow Fiber Membranes via Nonsolvent Induced Phase Separation, Chin. J. Chem. Eng., 20 (2012) 71-79.

[10] Y.-J. Guo, T. Long, W. Chen, C.-Q. Ning, Z.-A. Zhu, Y.-P. Guo, Bactericidal property and biocompatibility of gentamicin-loaded mesoporous carbonated hydroxyapatite microspheres, Mater. Sci. Eng., C, 33 (2013) 3583-3591.

[11] C.S. Ciobanu, S.L. Iconaru, I. Pasuk, B.S. Vasile, A.R. Lupu, A. Hermenean, A. Dinischiotu, D. Predoi, Structural properties of silver doped hydroxyapatite and their biocompatibility, Mater. Sci. Eng., C, 33 (2013) 1395-1402.

[12] M.A.F. Afzal, P. Kesarwani, K.M. Reddy, S. Kalmodia, B. Basu, K. Balani, Functionally graded hydroxyapatite-alumina-zirconia biocomposite: Synergy of toughness and biocompatibility, Mater. Sci. Eng., C, 32 (2012) 1164-1173.

[13] P. Robinson Ii, C. Wilson Ii, J. Mecholsky Jr, Processing and mechanical properties of hydroxyapatite–polysulfone laminated composites, J. Eur. Ceram. Soc., 34 (2014) 1387-1396.

[14] Z. Fang, Q. Feng, Improved mechanical properties of hydroxyapatite whisker-reinforced poly(l-lactic acid) scaffold by surface modification of hydroxyapatite, Mater. Sci. Eng., C, 35 (2014) 190-194.

[15] J. Sun, L. Wu, Polyether sulfone/hydroxyapatite mixed matrix membranes for protein purification, Appl. Surf. Sci., 308 (2014) 155-160.

[16] N. Ma, Y. Zhang, X. Quan, X. Fan, H. Zhao, Performing a microfiltration integrated with photocatalysis using an Ag-TiO2/HAP/Al2O3 composite membrane for water treatment: Evaluating effectiveness for humic acid removal and anti-fouling properties, Water Res., 44 (2010) 6104-6114.

[17] S. Masmoudi, R. Ben Amar, A. Larbot, H. El Feki, A.B. Salah, L. Cot, Elaboration of inorganic microfiltration membranes with hydroxyapatite applied to the treatment of wastewater from sea product industry, J. Membr. Sci., 247 (2005) 1-9.

[18] W.-Z. Lang, Q. Ji, J.-P. Shen, Y.-J. Guo, L.-F. Chu, Modified poly(vinylidene fluoride) hollow fiber composite membranes reinforced by hydroxyapatite nanocrystal whiskers, J. Appl. Polym. Sci., 127 (2013) 4564-4572.

[19] S. Zhang, R. Wang, S. Zhang, G. Li, Y. Zhang, Treatment of wastewater containing oil using phosphorylated silica nanotubes (PSNTs)/polyvinylidene fluoride (PVDF) composite membrane, Desalination, 332 (2014) 109-116.

[20] J. Hong, Y. He, Polyvinylidene fluoride ultrafiltration membrane blended with nano-ZnO particle for photo-catalysis self-cleaning, Desalination, 332 (2014) 67-75.

[21] X. Zhang, W.-Z. Lang, H.-P. Xu, X. Yan, Y.-J. Guo, L.-F. Chu, Improved performances of PVDF/PFSA/O-MWNTs hollow fiber membranes and the synergism effects of two additives, J. Membr. Sci., 469 (2014) 458-470.

[22] X. Li, R. Pang, J. Li, X. Sun, J. Shen, W. Han, L. Wang, In situ formation of Ag nanoparticles in PVDF ultrafiltration membrane to mitigate organic and bacterial fouling, Desalination, 324 (2013) 48-56.

[23] H. Shi, F. Liu, L. Xue, Fabrication and characterization of antibacterial PVDF hollow fibre membrane by doping Ag-loaded zeolites, J. Membr. Sci., 437 (2013) 205-215.

[24] Y. Wei, H.-Q. Chu, B.-Z. Dong, X. Li, S.-J. Xia, Z.-M. Qiang, Effect of TiO2 nanowire addition on PVDF ultrafiltration membrane performance, Desalination, 272 (2011) 90-97.

[25] E. Yuliwati, A.F. Ismail, T. Matsuura, M.A. Kassim, M.S. Abdullah, Effect of modified PVDF hollow fiber submerged ultrafiltration membrane for refinery wastewater treatment, Desalination, 283 (2011) 214-220.

[26] L.-Y. Yu, Z.-L. Xu, H.-M. Shen, H. Yang, Preparation and characterization of PVDF–SiO2 composite hollow fiber UF membrane by sol–gel method, J.Membr. Sci., 337 (2009) 257-265.

[27] X. Cao, J. Ma, X. Shi, Z. Ren, Effect of TiO2 nanoparticle size on the performance of PVDF membrane, Appl. Surf. Sci., 253 (2006) 2003-2010.

[28] L. Yan, Y.S. Li, C.B. Xiang, Preparation of poly(vinylidene fluoride)(pvdf) ultrafiltration membrane modified by nano-sized alumina (Al2O3) and its antifouling research, Polymer, 46 (2005) 7701-7706.

[29] T.-H. Bae, T.-M. Tak, Effect of TiO2 nanoparticles on fouling mitigation of ultrafiltration membranes for activated sludge filtration, J. Membr. Sci., 249 (2005) 1-8.

[30] W.-Z. Lang, Z.-L. Xu, H. Yang, W. Tong, Preparation and characterization of PVDF–PFSA blend hollow fiber UF membrane, J. Membr. Sci., 288 (2007) 123-131.

[31] W.-Z. Lang, Y.-J. Guo, L.-F. Chu, Evolution of the precipitation kinetics, morphologies, permeation performances, and crystallization behaviors of polyvinylidenefluoride (PVDF) hollow fiber membrane by adding different molecular weight polyvinylpyrrolidone (PVP), Polym. Adv. Technol., 22 (2011) 1720-1730.

[32] S. Zinadini, A.A. Zinatizadeh, M. Rahimi, V. Vatanpour, H. Zangeneh, Preparation of a novel antifouling mixed matrix PES membrane by embedding graphene oxide nanoplates, J. Membr. Sci.,

453 (2014) 292-301.

[33] V. Vatanpour, S.S. Madaeni, R. Moradian, S. Zinadini, B. Astinchap, Novel antibifouling nanofiltration polyethersulfone membrane fabricated from embedding TiO2 coated multiwalled carbon nanotubes, Sep. Purif. Tech., 90 (2012) 69-82.

[34] W.-Z. Lang, J.-P. Shen, Y.-T. Wei, Q.-Y. Wu, J. Wang, Y.-J. Guo, Precipitation kinetics, morphologies, and properties of poly(vinyl butyral) hollow fiber ultrafiltration membranes with respect to polyvinylpyrrolidone molecular weight, Chem. Eng. J., 225 (2013) 25-33.

[35] W.-Z. Lang, J.-P. Shen, Y.-X. Zhang, Y.-H. Yu, Y.-J. Guo, C.-X. Liu, Preparation and characterizations of charged poly(vinyl butyral) hollow fiber ultrafiltration membranes with perfluorosulfonic acid as additive, J. Membr. Sci., 430 (2013) 1-10.

[36] H. Zhang, K. Lamnawar, A. Maazouz, Rheological Modeling of the Mutual Diffusion and the Interphase Development for an Asymmetrical Bilayer Based on PMMA and PVDF Model Compatible Polymers, Macromolecules, 46 (2012) 276-299.

[37] D. Wu, J. Wang, M. Zhang, W. Zhou, Rheology of Carbon Nanotubes–Filled Poly(vinylidene fluoride) Composites, Ind. Eng. Chem. Res., 51 (2012) 6705-6713.

[38] H. Ma, Y. Yang, Rheology, morphology and mechanical properties of compatibilized poly(vinylidene fluoride) (PVDF)/thermoplastic polyurethane (TPU) blends, Polym. Test., 27 (2008) 441-446.

[39] S.H. Yoo, J.H. Kim, J.Y. Jho, J. Won, Y.S. Kang, Influence of the addition of PVP on the morphology of asymmetric polyimide phase inversion membranes: effect of PVP molecular weight, J. Membr. Sci., 236 (2004) 203-207.

[40] B. Chakrabarty, A.K. Ghoshal, M.K. Purkait, Preparation, characterization and performance

studies of polysulfone membranes using PVP as an additive, J. Membr. Sci., 315 (2008) 36-47.

[41] J. Zhang, Z. Xu, M. Shan, B. Zhou, Y. Li, B. Li, J. Niu, X. Qian, Synergetic effects of oxidized carbon nanotubes and graphene oxide on fouling control and anti-fouling mechanism of polyvinylidene fluoride ultrafiltration membranes, J. Membr. Sci., 448 (2013) 81-92.

[42] R. Miao, L. Wang, Y. Lv, X. Wang, L. Feng, Z. Liu, D. Huang, Y. Yang, Identifying polyvinylidene fluoride ultrafiltration membrane fouling behavior of different effluent organic matter fractions using colloidal probes, Water Res., 55 (2014) 313-322.

[43] I.H. Huisman, P. Prádanos, A. Hernández, The effect of protein–protein and protein–membrane interactions on membrane fouling in ultrafiltration, J. Membr. Sci., 179 (2000) 79-90.

[44] C. Zhao, X. Xu, J. Chen, F. Yang, Effect of graphene oxide concentration on the morphologies and antifouling properties of PVDF ultrafiltration membranes, J. Environ.Chem.Eng, 1 (2013) 349-354.

[45] W.-Z. Lang, X. Zhang, J.-P. Shen, H.-P. Xu, Z.-L. Xu, Y.-J. Guo, The contrastive study of chemical treatment on the properties of PVDF/PFSA and PVDF/PVP ultrafiltration membranes, Desalination, 341 (2014) 72-82.

[46] S. Yu, W. Zheng, W. Yu, Y. Zhang, Q. Jiang, Z. Zhao, Formation Mechanism of β-Phase in PVDF/CNT Composite Prepared by the Sonication Method, Macromolecules, 42 (2009) 8870-8874.

[47] K. Lin, L. Chen, P. Liu, Z. Zou, M. Zhang, Y. Shen, Y. Qiao, X. Liu, J. Chang, Hollow magnetic hydroxyapatite microspheres with hierarchically mesoporous microstructure for pH-responsive drug delivery, Cryst Eng Comm, 15 (2013) 2999.

[48] T. Li, G. Zhong, R. Fu, Y. Yang, Synthesis and characterization of Nafion/cross-linked PVP semi-interpenetrating polymer network membrane for direct methanol fuel cell, J. Membr. Sci., 354

(2010) 189-197.

[49] T. Boccaccio, A. Bottino, G. Capannelli, P. Piaggio, Characterization of PVDF membranes by vibrational spectroscopy, J. Membr. Sci., 210 (2002) 315-329.

[50] F. Ye, H. Guo, H. Zhang, Biomimetic synthesis of oriented hydroxyapatite mediated by nonionic surfactants, Nanotechnology, 19 (2008) 245605.

[51] L. Chen, C.Y. Tang, C.P. Tsui, D.Z. Chen, Mechanical properties and in vitro evaluation of bioactivity and degradation of dexamethasone-releasing poly-d-l-lactide/nano-hydroxyapatite composite scaffolds, J. Mech. Behav. Biomed. Mater., 22 (2013) 41-50.

[52] A. Bianco, E. Di Federico, I. Moscatelli, A. Camaioni, I. Armentano, L. Campagnolo, M. Dottori, J.M. Kenny, G. Siracusa, G. Gusmano, Electrospun poly(ε-caprolactone)/Ca-deficient hydroxyapatite nanohybrids: Microstructure, mechanical properties and cell response by murine embryonic stem cells, Mater. Sci. Eng., C, 29 (2009) 2063-2071.

[53] H. Kim, L.H. Che, Y. Ha, W. Ryu, Mechanically-Reinforced Electrospun Composite Silk Fibroin Nanofibers Containing Hydroxyapatite Nanoparticles, Mater. Sci. Eng., C 40(2014)324-335.

Table captions

Table 1 The published works about the properties of PVDF membranes modified by inorganic additives

Table 2 The detailed preparation conditions of PVDF/PVP/HAP hollow fiber membranes

Table 3 The geometrical parameters of PVDF/PVP/HAP hollow fiber membranes

Table 4 The quantitative summary of the surface roughness of M-1~M-4

Table 5 Permeation and rejections of PVDF/PVP/HAP membranes

Table 6 Mechanical properties of PVDF/PVP/HAP hollow fiber membranes

Figure captions

Fig.1 The viscosity versus shear rate of PVDF/PVP/HAP dopes

Fig.2 Effect of HAP content on the precipitation kinetics of PVDF/PVP/HAP dope solutions

Fig.3 FESEM images of the cross-sectional morphologies of PVDF/PVP/HAP hollow fiber membranes

Fig.4 FESEM images of the outer surfaces of PVDF/PVP/HAP hollow fiber membranes

Fig.5 FESEM images of the inner surfaces of PVDF/PVP/HAP hollow fiber membranes

Fig.6 EDX map scanning spectra for the outer surface of M-2

Fig.7 The brief illustration of the interactions between PVP and HAP

Fig.8 AFM images of the outer surfaces of PVDF/PVP/HAP hollow fiber membranes

Fig.9 The dynamic contact angles of PVDF/PVP/HAP hollow fiber membranes

Fig.10 Permeation flux for different protein solutions in terms of running time

Fig.11 Time-dependent flux of PVDF/PVP/HAP hollow fiber membranes with 3 ultrafiltration and cleaning cycles

Fig.12 XRD patterns of PVDF/PVP/HAP hollow fiber membranes and HAP whiskers

Fig.13 ATR-FTIR spectra of PVDF/PVP/HAP hollow fiber membranes